Thermochimica Acta 720 (2023) 179421

Contents lists available at ScienceDirect

Thermochimica Acta

journal homepage: www.elsevier.com/locate/tca

# Combustion characteristics of lithium perchlorate-based electrically controlled solid propellants at elevated pressures

Kanagaraj Gnanaprakash [a,b], Daehong Lim [a], Jack J. Yoh [a,*]

[a] Department of Aerospace Engineering, Seoul National University, Seoul 08826, Republic of Korea
[b] Department of Mechanical and Aerospace Engineering, Indian Institute of Technology Hyderabad, Kandi, Telangana 502284, India

ARTICLE INFO

*Keywords:*
Electrically controlled solid propellants
Lithium perchlorate
Multi-wavelength pyrometry
Ignition delay time
Pyroelectric combustion

ABSTRACT

Electrically controlled solid propellants (ECSPs) exhibit specific combustion characteristics that offer multiple start/stop operations and variable combustion rates at different electrical power. The present study investigates ignition and pyroelectric combustion characteristics of ECSPs, based on lithium perchlorate (LP) oxidizer and poly vinyl alcohol (PVA) binder, in the elevated pressure range of 0.1 to 2.0 MPa, and to further understand the performance of tungsten (W) as a metal additive. Experiments are conducted for metallized ECSPs with 5% (M5), 10% (M10) and 15% (M15) W content, relative to the non-metallized case. Ignition delay time ($T_{ign}$) for the baseline (M0) decreased substantially from 633 ms at 0.1 MPa to 178 ms at 2.0 MPa pressure. A similar decreasing trend for the minimum electrical energy required for ignition was also observed with increase in pressure. Addition of W decreased $T_{ign}$ and electrical ignition energy significantly by 33% and 66% respectively, for M15 relative to M0. Furthermore, thermochemical equilibrium analysis indicated that the adiabatic combustion temperature and specific impulse decreased with increase in W content due to increased fuel-rich stoichiometry. Overall, the metal addition significantly enhanced the combustion rates at all pressure range below 2.0 MPa. It is anticipated that the observed characteristics at elevated pressures provide insights into the design of electrically-controlled operations for future propulsion systems.

## 1. Introduction

Electrically controlled solid propellants (ECSPs) undergo combustion only when sufficient electric power is supplied and completely extinguish in the absence of this external electrical source [1,2], the feature known as pyroelectric combustion behaviour. By applying the same electrical power, re-ignition can be achieved again. This specific feature permits these propellants to establish discrete impulse bits and multiple start/stop operations. Combustion rate of these propellants can be varied significantly by changing the external electrical power under pressurized conditions. Due to their excellent performance including high stability, controllable throttle, multiple ignitions and extinguishments, ECSPs can be widely utilized from micro to macro propulsion systems, such as small satellites, pulsed plasma thrusters, gas generator systems, long range rocket motors, etc. [2]. In addition, ECSPs are insensitive to external stimulus such as sparks, impact, electrostatic discharge, or even open flame [3].

A typical ECSP formulation consisted of an ionic liquid/oxidizer such as hydroxyl ammonium nitrate (HAN) or lithium perchlorate (LP), a polymer binder such as poly vinyl alcohol (PVA), and a cross-linking agent. Other ingredients such as metal additives, burn rate modifiers, plasticizers, and stabilizers are included in formulations to improve their ballistic performance and mechanical properties to meet specific mission requirements. Many studies have reported about thermal decomposition, thermochemistry and combustion process involved with HAN/PVA based ECSPs in the past [4–7]. Recently, Glascock et al. [6] have studied about the utilization of above propellants in an ablative pulsed plasma thruster, and obtained their impulse and performance measurements. Aluminum (Al) as metal additive in HAN-based ECSPs was considered by Bao et al. [7] to investigate the effect of different particle sizes and contents of Al on their ignition and combustion characteristics in the pressure range of 0.1 to 1.0 MPa. However, low decomposition temperature and hygroscopic nature of HAN oxidizer caused significant melting and smoldering at high temperatures with these propellants. This resulted in a poor thermal stability of HAN-based ECSPs [8,9]. In addition, these aluminized ECSPs exhibited self-sustained combustion above 1.0 MPa, which could deprive from their multiple start/stop capabilities and restrain their usage in specific

* Corresponding author.
*E-mail address:* jjyoh@snu.ac.kr (J.J. Yoh).

https://doi.org/10.1016/j.tca.2022.179421
Received 31 October 2022; Received in revised form 14 December 2022; Accepted 15 December 2022
Available online 16 December 2022

applications.

In order to improve the thermal stability of ECSPs, recent studies have replaced HAN by LP, as the ionic oxidizer, and investigated their thermal decomposition and combustion behaviour [9–11]. Wang et al. [8] have shown a strong dependence of burning rates on ionic conductivity of polyethylene oxide-polyacrylonitrile based ion conductive energetic composites, considered as replacement for HAN-based aluminized ECSPs. In other study, He et al. [9] presented that LP/PVA/Al-based ECSPs indicate increased burning rates with increase in the electrical voltage and ambient pressure in the range from 0.2 to 5.0 MPa. Some studies have considered tungsten (W) as metal additive and reported improvement in thermal decomposition and performance characteristics of these propellants [11,12]. Since the volumetric energy density (~85 kJ/cm$^3$) of W is similar to Al [13], and the thermal conductivity is comparable between these two metals, W can also be considered as a potential alternate metal additive for ECSPs.

Most works on ECSPs have focussed mainly on HAN-based propellants and elucidated their fundamental decomposition and combustion mechanisms at low pressures. Only a few studies have focussed on investigating the ignition and combustion behaviour of different types of ECSPs at high pressures [8,9,14,15]. Zamir et al. [15] have reported increasing burning rates of ammonium nitrate-epoxy based ECSPs with pressure up to 5.0 MPa and with electrical voltage up to 250 V. Research on LP-based ECSPs attempted to examine their ignition and combustion behaviour are scant in the literature. In addition, governing reaction mechanisms of these ECSPs are not completely understood. This is mainly due to their complex physicochemical processes, electrochemistry coupled with thermo-chemical reactions, multiphase heat and mass transfer, etc.

In the present study, ignition and combustion characteristics of metallized LP-based ECSPs are investigated in the pressure range of 0.1 to 2.0 MPa, in comparison to the non-metallized case. The influence of tungsten as a metal additive at three different contents is examined as well. Theoretical performance calculations for these ECSP formulations are performed using thermochemical equilibrium code. Experiments are conducted to obtain the ignition delay time, electrical energy required for ignition/combustion, combustion temperature, and pyroelectric combustion rates of non-metallized ECSP and W-based ECSPs at elevated pressures.

## 2. Experimental section

### 2.1. Samples

The present study utilized lithium perchlorate (Alfa Aesar Ltd.) with purity of 99.0% as oxidizer, polyvinyl alcohol (Sigma-Aldrich Ltd.) with molecular weight in the range of 146,000-18,6000 and degree of hydrolysis of 99.0% as binder/fuel, tungsten (US Research Nanomaterials Inc.) with particle size of 1 μm as metal additive, boric acid ($H_3BO_3$) as cross-linking agent and glycerin as plasticizer. Glycerin was added particularly to improve the conductivity and electrochemical properties of PVA in the mixture [16]. In all cases, the original LP/water ratio was maintained as 1:1.85, which was slightly different from the actual solubility limit (1:1.67 at 25 °C) of LP in water, to achieve complete solubility and to improve the mixing process. The content of W was varied as 5%, 10% and 15% in the initial metallized formulations, wherein the weight percent of other ingredients and LP/water ratio were retained the same as the non-metallized baseline ECSP-M0. Table 1 shows initial compositions of different propellants before the curing process, and their final compositions after curing. It is seen that after the curing process, the water content in the final composition has changed due to evaporation, and correspondingly there was an increase in the weight percentage of other ingredients. These formulations were recalculated after presuming ~20% water to be present in final samples after curing, confirmed through mass loss analysis in our previous studies [11,17]. Note that the content of glycerin and boric acid was maintained as 4% and 2% respectively, in initial formulations of all ECSPs.

**Table 1**
Initial and final compositions of various ECSPs before and after the curing process.

| Samples | Ingredients content before/after curing | | | | | |
|---|---|---|---|---|---|---|
| | LP (%) | $H_2O$ (%) | PVA (%) | $H_3BO_3$ (%) | Glycerin (%) | W (%) |
| ECSP-M0 | 29.47/51.85 | 54.53/20 | 10/17.59 | 2/3.52 | 4/7.04 | - |
| ECSP-M5 | 27.72/45.52 | 51.28/20 | 10/16.42 | 2/3.28 | 4/6.57 | 5/8.21 |
| ECSP-M10 | 25.96/39.97 | 48.04/20 | 10/15.40 | 2/3.08 | 4/6.16 | 10/15.40 |
| ECSP-M15 | 24.21/35.08 | 44.79/20 | 10/14.49 | 2/2.90 | 4/5.79 | 15/21.74 |

The propellant preparation procedure was described in our previous study [11]. Briefly, LP and PVA were first dissolved in the distilled water, and then mixed with glycerin followed by boric acid in the last step. For metallized samples, W was added to this mixture before the curing agent. A planetary centrifugal mixer (Thinky ARE-310, Japan) was employed for mixing the ingredients and degassing the mixture for ~30 min. A highly viscous homogeneous propellant slurry was obtained without any voids after mixing, which was then cured into soft rubbery solid in a hot air oven at 35 °C for 5–7 days. Cured propellant samples were cut into strands of dimensions of 6-8mm × 4mm × 4mm with an average mass of ~145 mg and utilized for ignition/combustion studies. Note that the density of W (19.35g/cm$^3$) is considerably high, which could cause the high-density W in the propellant slurry (with ~50% water content) to settle down at the bottom of container in the initial stage of curing. Despite this, settling down of W particles was not observed with the end-of-mix propellant slurry, since significant quantity of water had already evaporated during mixing. Moreover, this problem was avoided by rotating the propellant container upside down at regular time intervals. Recall that the final water content in cured ECSPs was different from their initial formulations since a large amount of water evaporated in the curing process, which slightly reduced the overall volume of cured propellants.

### 2.2. Methods

Combustion experiments were performed inside a windowed strand burner in the pressure range from 0.1 to 2.0 MPa, by utilizing a combustion test stand and regulated DC power supply (1 kV and 1 A). This experimental facility is depicted in Fig. 1. The volume of the strand burner is substantially larger than the propellant volume, so that the chamber pressure is not significantly affected by product gases from propellant combustion. The chamber was pressurized with nitrogen gas and regulated with a pressure regulator to achieve different pressure levels. The combustion test stand consists of a set of electrodes made up of molybdenum (10mm × 20mm × 5mm), support stands, and wire connections for applying input power to the propellant. The propellant was placed in between the electrodes in a vertical burning configuration such that the freely movable top electrode was positive, and the bottom electrode was negative, similar to our previous study [17]. Since the area ratio of the anode to cathode is 1:1, in this study, the anode is where electrically triggered combustion occurs most favorably [18]. Varying the area ratio of the electrode pairs stimulates the combustion to occur at the smaller electrode irrespective of the cathode or anode, implying that the burning is independent of the polarity [1,18].

When external power was applied, initially ignition and then pyroelectric combustion occurred at the top positive electrode that displaced downwards in the vertical direction due to gravity. This displacement ensured that the top electrode was in continuous contact with the burning surface since the electrodes must always be touching the propellant for further uninterrupted combustion. Thrust produced by the

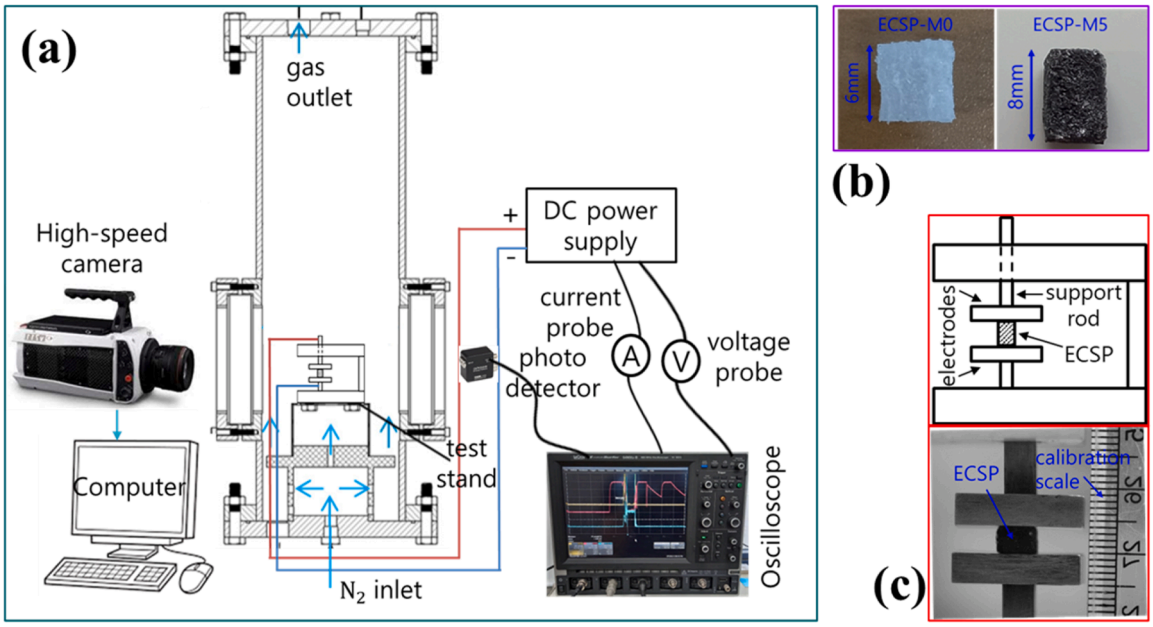


**Fig. 1.** Schematic of the experimental setup (a), photographs of ECSP-M0 and ECSP-M5 (b) and enlarged view of the combustion test stand (c).

small ECSP sample is too small at the considered pressures, and the weight of the electrode is relatively higher than the weight of the ECSP sample which ensures that there is no part of the combustion where the contact of the electrode is completely absent during the combustion. But this can result in the slight oscillations in the voltage and the current data which is utterly anticipated and acceptable as this study has the intent to report the mean burning rate data. The above vertical configuration was considered to obtain the ignition and combustion characteristic parameters of ECSPs at different pressures of 0.1, 0.5, 1.0, 1.5 and 2.0 MPa. For all these tests, the initial applied voltage and current were maintained at 300 V and 1 A in the DC power supply. Hence, in this study, only the effect of the mean chamber pressure on the combustion rate of ECSP's are reported and not the effect of the changing voltage and current as it is maintained constant for all the experiments. The main intent of this paper is to establish and show the effect of pressure on the combustion rates of ECSPs.

Instantaneous variations in applied input power to the propellant were recorded through voltage and current probes, using a four-channel digital oscilloscope (LeCroy, WaveSurfer 64MXs-B, 600 MHz bandwidth, rate of 10 GS/s). The voltage probe was purchased from Hantek company (T3100, 100 MHz bandwidth, attenuation of 100:1), and the current probe was procured from Tektronix Inc. (A622, 100 kHz bandwidth, output scale of 100 mV/A). In addition, a Si-based photodetector (Thorlabs, DET025A/M, 2 GHz bandwidth, 400-1100 nm range) was attached to the outside of window of the burner to acquire the light intensity data during the ignition and combustion event of these propellants, which was then recorded in the oscilloscope. In particular, it is focused more on collecting signals from the initial ignition of the propellant than signals from steady combustion, due to the limitation of the experimental structure. All three data from photodetector, voltage probe, and current probe were recorded separately in each channel of the oscilloscope at the sampling rate of 1 kS/s.

When the power supply was turned on, voltage and current signals commenced to increase as seen from the oscilloscope, and then propellant ignition/combustion occurred after a time delay. The photodetector immediately started acquiring the luminous intensity signal from the propellant burning surface. Therefore, the ignition delay time ($T_{ign}$) was calculated as the difference between the onset of current signal rise and the onset of photodetector signal rise. Simultaneously, this combustion event was captured using a high-speed camera (Phantom V711, with resolution of 800 × 600 pixels$^2$) fitted with a 105 mm Nikkor macro lens [19], at a framing rate of 100 fps and exposure time from 500-3000 μs depending on propellant formulations. In this study, a flat plate vertical burning configuration was utilized, wherein the propellant was always in contact with the electrodes. The burn away of the propellant surface displaced the top electrode downwards at the same rate as propellant regression. Because of high radiation intensity from the flame/combustion zone, pixels near the actual propellant burning surface were saturated in combustion images and it was highly challenging to locate the exact burning surface. Therefore, locus points of displacement of the moving top electrode in burning images were measured in the real time and plotted against the time to get the displacement rate, instead of tracking the actual regressing propellant surface. This displacement rate of the top electrode was presumed to be the same as the propellant combustion rate. The slope was almost constant during combustion of each sample, implying that steady combustion was achieved. In general, these displacement points were obtained at 2 or more different locations across the sample cross section to obtain corresponding burning rate values at those locations. Then, the mean and deviation of these 2 or more burning rate values from a single sample, burning at a specific pressure, was plotted in the burning rate against pressure plots (Section 3.3). Separate custom MATLAB codes were utilized to obtain $T_{ign}$ and combustion rates from oscilloscope data and burning images respectively, for different ECSPs. All combustion tests were repeated at least twice for each propellant composition at different pressures. The uncertainty in the measurement of $T_{ign}$ was within ±5% and that of each burning rate data from a particular test was within ±3%.

Furthermore, the radiation spectrum emitted from propellant burning was utilized for measuring the combustion temperature of ECSP-M5 and ECSP-M10 samples under ambient conditions, using multi-wavelength pyrometry [20,21]. This intensity spectrum was captured with a spectrometer (Dongwoo optron, MonoRa320i) and intensified charged coupled device (ICCD) camera (Andor, IStar). The acquisition rate for the spectrometer was set as 1 kHz, which was the maximum rate achievable with the camera for the current experimental conditions. A doublet pair optics (Thorlabs, MAP10100100-A) and fiber optic cables (Ocean optics, QP200-2-UV-BX, 200 μm diameter) were installed between the region of interest on the propellant surface and spectrometer, in order to obtain point measurements with a focus area of

200 μm. This point measurement corresponds to a position at 1.5 mm from the propellant bottom and located at the center of its width. Before performing pyrometry experiments, the calibration was conducted. Fig. 2 shows the response difference between the tungsten-halogen lamp (SL1-CAL, 2800 K) and the pyrometer, because of which the transfer function for the entire measuring range of the wavelength was applied. The manual calibration for non-linearity of the response was not necessary in this study, since the calibration between ICCD and spectrometer was done via the software.

## 3. Results and discussion

### 3.1. Theoretical performance calculations

Thermochemical equilibrium calculations were performed for different W based ECSP compositions considered in the present study by using the Cheetah 4.0 thermochemical code [22], under the conditions of 7.0 MPa chamber pressure, 0.1 MPa exit pressure, and 25°C ambient temperature. These propellant compositions were recalculated after assuming ~20% water to be present in those samples [11]. Results obtained for specific impulse ($I_{sp}$), adiabatic combustion temperature ($T_{ad}$), and concentration of different products are presented in Fig. 3 for various ECSPs, wherein the metal content was varied as 0%, 5%, 10% and 15% for these cases [17].

For W based ECSPs, $T_{ad}$ and $I_{sp}$ indicate lower values than the non-metallized baseline case (ECSP-M0) and a decreasing trend with increase in the metal content in propellant formulations (Fig. 3a). In products composition (Fig. 3b), a considerable amount of $H_2O$ and $CO_2$ is noticed for all cases, and the metal oxide ($WO_3$) is observed to be in solid phase. This suggests that the oxidation of W metal particles is limited and could have occurred mostly in the condensed phase, which decreased the theoretical combustion temperature as the metal content is increased in these compositions. In addition, large amounts of high molecular weight compounds are seen in products rather than lighter compounds such as $H_2$ and CO. Therefore, the presence of heavier products and decreasing combustion temperature with increase in the metal content induced a decreasing trend for $I_{sp}$ as well, for W based formulations. Also, the total products concentration ($C_{prod}$) decreased with increase in the metal content (Table 2), indicating further unreacted reactants with these ECSPs.

Note that the baseline ECSP-M0 composition has slightly excess oxidizer in products, implying that its stoichiometry is oxidizer-rich. However, all metallized compositions show presence of excess fuel in their products, thus suggesting a fuel-rich stoichiometry for these ECSPs. The equivalence ratio ($\phi$) for these formulations corroborates the same increasing fuel-rich stoichiometry, as presented in Table 2. Increased oxygen requirement for W oxidation with increasing fuel-rich stoichiometry of ECSPs with large metal content caused reduction in the theoretical performance and increase in condensed phase products. However, it is realized from our previous work [11,17] and in the present study that the presence of W incorporates significant influence on the combustion behaviour in terms of substantial increment in combustion rates of these ECSPs, as will be shown later.

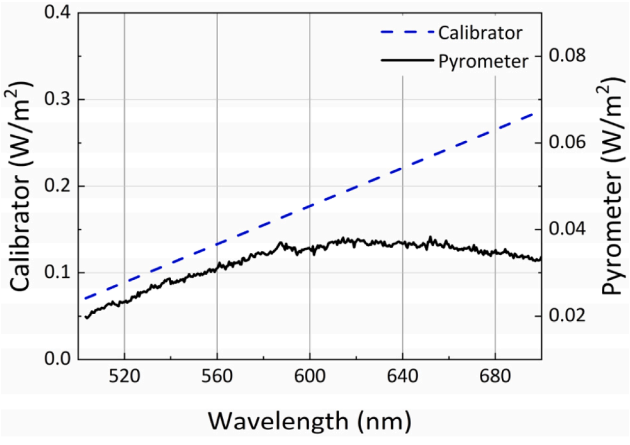


**Fig. 2.** Response difference between tungsten-halogen lamp calibrator and pyrometer.

### 3.2. Influence of pressure on ignition characteristics of ECSPs

Experiments were conducted inside the windowed strand burner to obtain the ignition delay time ($T_{ign}$) and pyroelectric combustion rates simultaneously, under 300 V and 1 A electrical power, in the pressure range of 0.1 to 2.0 MPa for various ECSPs considered in this study. The measurements of current ($A$), voltage ($V$) and luminous intensity ($I$) from photodetector due to propellant burning were recorded in the digital oscilloscope. From this, the ignition delay time was evaluated based on the difference between the onset of rise of radiation intensity signal ($t_1$) and the onset of rise of current signal ($t_0$). Resistance offered by the propellant and the energy required for ignition/combustion process were also calculated from $V$ and $A$ data as indicated. The initial value of resistance ($R$) and electrical energy ($E$) was considered at $t_0$ since electrical current started to rise only from this time instance. The overall trend of the above parameters remained the same for all cases, wherein the current transmission to propellants was initiated at $t_0$. Represented plots of $V$, $A$, and $I$ measurements and calculated $R$ and $E$ are shown in Fig. 4, for baseline ECSP-M0 and ECSP-M15 at 1.0 MPa pressure. $R$ and $E$ variations are plotted against time starting from $t_0$ during the initial ignition transient period.

The time at $t_0$ represents that the baseline ECSP-M0 has started to conduct current from the top positive electrode to the bottom negative electrode, after switching on the DC power source. In this period, the resistance offered by the propellant has decreased significantly, whereas the electrical energy has increased. Following a slight time delay, ignition is achieved in the propellant as seen by the rise of intensity signal from the photodetector at time $t_1$ (Fig. 4a). The electrical energy provided to the propellant at this time instance $t_1$ is determined to be the minimum ignition energy (190 J) of ECSP-M0 from Fig. 4b, which is less than maximum electrical energy supplied to propellants since it continued to increase beyond 200 J during the combustion process. Note that the external energy is required uninterruptedly even after ignition to sustain combustion with ECSP-M0 in the entire pressure range. When the electrical power was removed, propellant burning ended. Furthermore, the voltage ad current signals were observed to be oscillating near the end of propellant burning, implying that the contact between the propellant and electrodes may not be uniform. This could cause difficulty in reignition of these propellants after the first cycle of burning when utilized for multiple start-stop operations and needs to be addressed in detail in future studies.

With the addition of W, the minimum ignition energy for ECSP-M15 with 15% W content was considerably reduced (80 J), relative to ECSP-M0. The average and standard deviation of minimum ignition energy obtained for different cases at 1.0 MPa are listed in Table 3. This indicates that increase in W content in ECSPs progressively reduced the minimum electrical energy required for ignition. In addition, high pressure also has similar effect of lowered electrical energy for ignition/combustion of baseline and metallized propellants. The energy required for igniting ECSP-M0 reduced considerably when operating at high pressures (98 J at 2.0 MPa). This is noticed with the resistance and energy plot obtained at 2.0 MPa for ECSP-M0, shown in the supplementary (Fig. S1).

The ignition delay time obtained at different pressures for ECSP-M0 in comparison to metallized ECSPs is plotted in Fig. 5. It is apparent that $T_{ign}$ decreased substantially when pressure is increased from 0.1 MPa to 2.0 MPa for all cases. For ECSP-M0, $T_{ign}$ decreased from 633 ms at 0.1 MPa to 272 ms at 0.5 MPa (by 57%), which further reduced to 178 ms

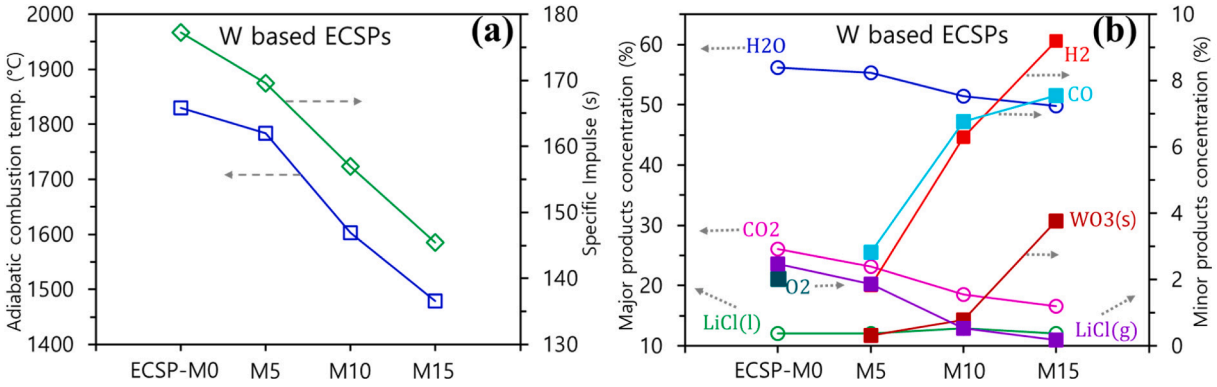


**Fig. 3.** Theoretical performance parameters for W based ECSPs with increasing metal content, in comparison to the non-metallized case. (a) Tad and Isp, (b) Cprod.

**Table 2**
Comparison of theoretical performance results of various ECSPs.

| Samples | $T_{ad}$ (°C) | $I_{sp}$ (s) | $C_{prod}$ (mol/kg) | $H_2O$ (%) | $CO_2$ (%) | $H_2$ (%) | CO (%) |
|---|---|---|---|---|---|---|---|
| ECSP-M0 ($\phi$ = 0.97) | 1830 | 177.3 | 34.1 | 56.1 | 26.1 | - | - |
| ECSP-M5 ($\phi$ = 1.04) | 1784 | 169.6 | 31.5 | 55.5 | 23.3 | 1.8 | 2.9 |
| ECSP-M10 ($\phi$ = 1.11) | 1603 | 157.0 | 30.2 | 51.4 | 18.6 | 6.3 | 6.8 |
| ECSP-M15 ($\phi$ = 1.19) | 1479 | 145.4 | 29.6 | 49.8 | 16.6 | 9.2 | 7.6 |

$\phi$ – Equivalence ratio; $T_{ad}$ – adiabatic combustion temperature; $I_{sp}$ – specific impulse; $C_{prod}$ – total concentration of products

(by 72%) as the pressure is increased up to 2.0 MPa. For metallized ECSPs containing 5%, 10% and 15% W content, the results signify that $T_{ign}$ followed a similar trend with increase in pressure for each composition (Fig. 5b). Both ECSP-M5 and ECSP-M15 indicated a decrement in the ignition delay time by 65% in the full tested pressure range. This suggests that the ignition characteristics of baseline and metallized ECSPs are considerably improved due to the pressure effect, which is a common feature among composite solid propellants.

In addition, $T_{ign}$ also reduced steadily with increase in the metal content among metallized propellants at each pressure. For instance, $T_{ign}$ is diminished by 32% and 44% at 1.0 MPa and 2.0 MPa respectively, for ECSP-M15 in comparison to ECSP-M5. This is due to the increased electrical conductivity of metallized propellants caused by the presence of W particles. More metal content in ECSPs improves the bulk electrical conductivity as well as thermal conductivity of those samples, since

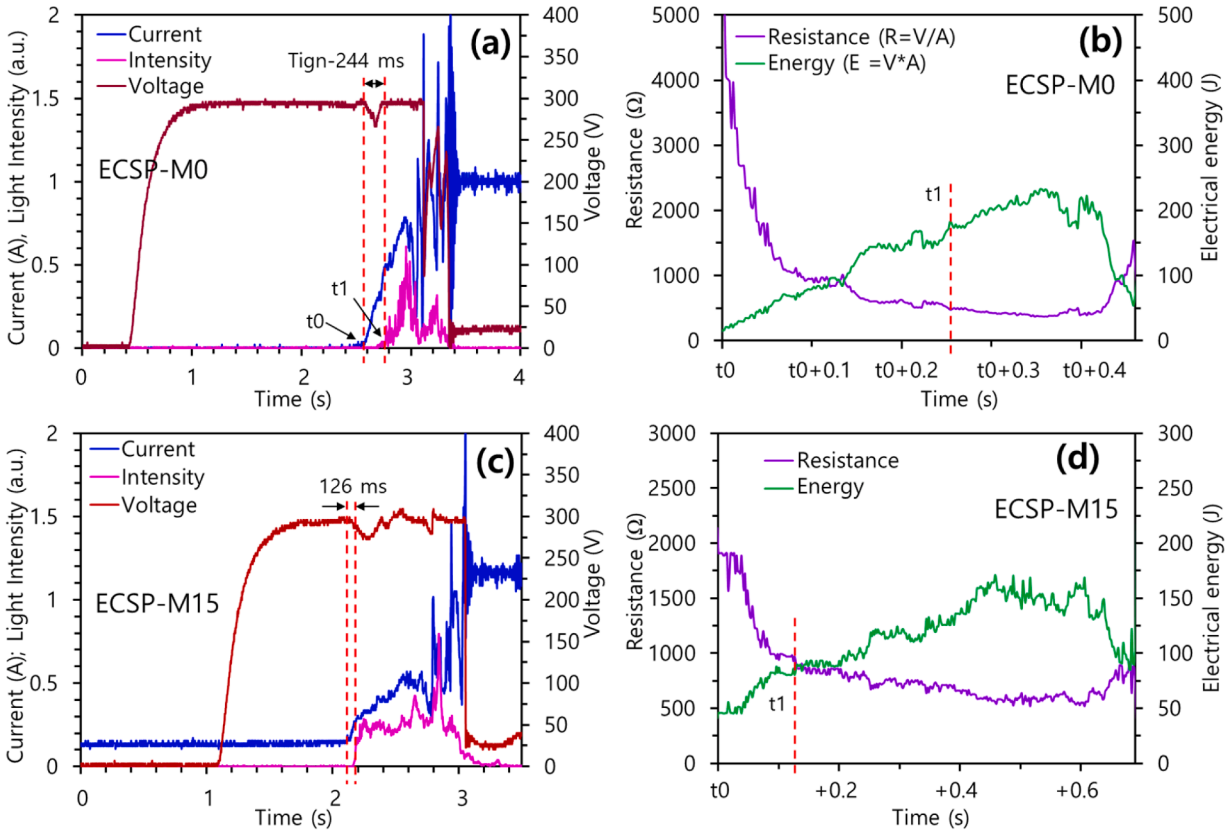


**Fig. 4.** Measurements of current, voltage and radiation intensity data, and calculated resistance & electrical energy from V and A data for ECSPs burning at 1.0 MPa. (a, b) ECSP-M0; (c, d) ECSP-M15.

**Table 3**
Different parameters from ignition characteristics and combustion rate plots of baseline ECSP-M0 and various metallized ECSPs.

| Sample | Ignition parameters at 1.0 MPa | | Mean combustion rate range (mm/s) | Power law constants ($r = aP^n$) | | |
|---|---|---|---|---|---|---|
| | Ignition delay time, $T_{ign}$ (ms) | Minimum electrical energy (J) | | Pressure exponent ($n$) | Temperature coefficient ($\log a$) | Correlation coefficient ($R^2$) |
| ECSP-M0 | 196±39 | 251±43 | 2.25 (0.1 MPa) 7.54 (2.0 MPa) | 0.39 | 2.22 | 0.87 |
| ECSP-M5 | 193±34 | 226±13 | 1.87 (0.1 MPa) 7.64 (2.0 MPa) | 0.47 | 2.05 | 0.87 |
| ECSP-M10 | 187±10 | 186±15 | 1.72 (0.1 MPa) 7.43 (2.0 MPa) | 0.50 | 1.91 | 0.82 |
| ECSP-M15 | 132±7 | 86±5 | 2.74 (0.1 MPa) 9.05 (2.0 MPa) | 0.38 | 2.83 | 0.84 |

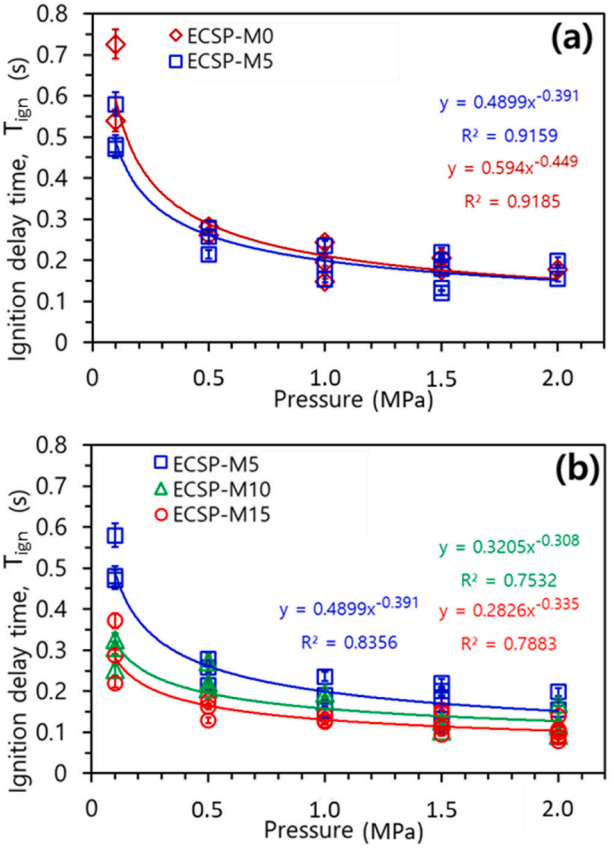


**Fig. 5.** Ignition delay time (Tign) as a function of pressure for metallized ECSPs in comparison to ECSP-M0 at external electrical power of 300 V and 1 A.

metal particles typically have higher conductivity than other ingredients. However, the metal content effect on $T_{ign}$ is marginal when compared to the pressure effect. Also, notice that $T_{ign}$ is almost the same between ECSP-M5 and baseline ECSP-M0 at pressures above 0.5 MPa (Fig. 5a). This implies that low metal content in these propellants does not influence the ignition delay time and minimum ignition energy significantly, although it alters the overall stoichiometry and equivalence ratio of propellant compositions, as mentioned before in Section 3.1. Furthermore, the standard deviation of $T_{ign}$ with these ECSPs tend to diminish considerably in high metal content formulations, as seen in Table 3 at 1.0 MPa. This suggests that more metal content with metallized propellants results in high stability of their ignition characteristics.

### 3.3. Influence of pressure on combustion behaviour of ECSPs

Independently, the multi-wavelength pyrometry technique [19,20] was performed under atmospheric conditions in order to measure the time-resolved combustion temperature of metallized ECSP-M5 and ECSP-M10. This method utilizes Planck's radiation law, shown in Eq. (1), which relates the spectral irradiance with temperature and wavelength of the light emitted from a substance. Here, $C_1 = 2hc^2$ and $C_2 = hc/k$ are known as Planck's first and second radiation constants, $h$ is the Planck's constant, $c$ is the velocity of light and $k$ is the Boltzmann's constant. Each of the emissivity at the specific wavelength and temperature, wavelength, and temperature are represented as $\varepsilon$, $\lambda$, and $T$, respectively. Similar to a previous study [21], the combustion temperature was measured by applying the measured radiance intensity into the modified Planck's radiation equation shown in Eq. (2). A derived quantity $y$ was introduced first to separate Eq. (1) into two parts, namely the measurement part and the temperature calculation part. Then the value $y$ was calculated from the raw intensity spectrum caused by the radiation of propellant burning and plotted against the wavelength. In the present study, the wavelength range was considered from 503 to 700 nm because of the device characteristics and emitted radiation spectrum. This raw intensity spectrum from the spectrometer at specific time instance along with the calibrated radiance and the derived quantity $y$ as a function of the wavelength are shown in Fig. 6, for ECSP-M5 burning at 0.1 MPa. In Fig. 6b, data points represented by black dots were calculated from the second part of Eq. (2), against each wavelength step, and it denotes a part of the measured intensity data from experiments. Likewise, the last part of Eq. (2) represents a fitted linear curve to be extracted from the second part (red straight line). Subsequently, the inverse of the combustion temperature was evaluated from the y-axis intercept of the straight line fitted to datapoints of the quantity $y$ according to Eq. (2).

$$E(\lambda,\ T) = \varepsilon(\lambda,\ T)\frac{C_1}{\lambda^5[e^{C_2/\lambda T}-1]}\ \text{(Planck's radiation equation)} \tag{1}$$

$$y = \frac{\lambda}{C_2}\ln\left(\frac{C_1}{\lambda^5}\frac{1}{E(\lambda,\ T)}\right) = \frac{1}{T} - \frac{\lambda}{C_2}\ln(\varepsilon(\lambda,\ T))\ \text{(Modified Planck's radiation equation)} \tag{2}$$

The time-resolved temperature distribution obtained from this analysis at different time instances during combustion of ECSP-M5 and ECSP-M10 at 0.1 MPa is shown in Fig. 7a. The corresponding average combustion temperatures and their standard deviation are depicted in Fig. 7b as a box plot. Furthermore, the theoretical adiabatic combustion temperature evaluated from Cheetah 4.0 (Section 3.1) are shown as straight lines in the figure for comparison. Results indicate that experimentally obtained temperatures are in good agreement with calculated theoretical values with slight deviation. For ECSP-M5, the thermochemical equilibrium code calculated an adiabatic temperature of 1784 K, which is similar to the average value of 1771 K extracted from multi-wavelength pyrometry. Likewise, ECSP-M10 exhibits average combustion temperatures of 1603 K and 1694 K obtained from calculations and experiments, respectively. In addition, it is shown that the equilibrium code could be employed to correctly predict the combustion temperature for various ECSP formulations. Moreover, a variation of 4.3% in combustion temperatures with increase in the metal content of ECSPs was within the data spread from this measurement. This signifies that more W content in propellant formulations resulted in limited oxidation of metal particles up to 10%. However, the improved bulk electrical and

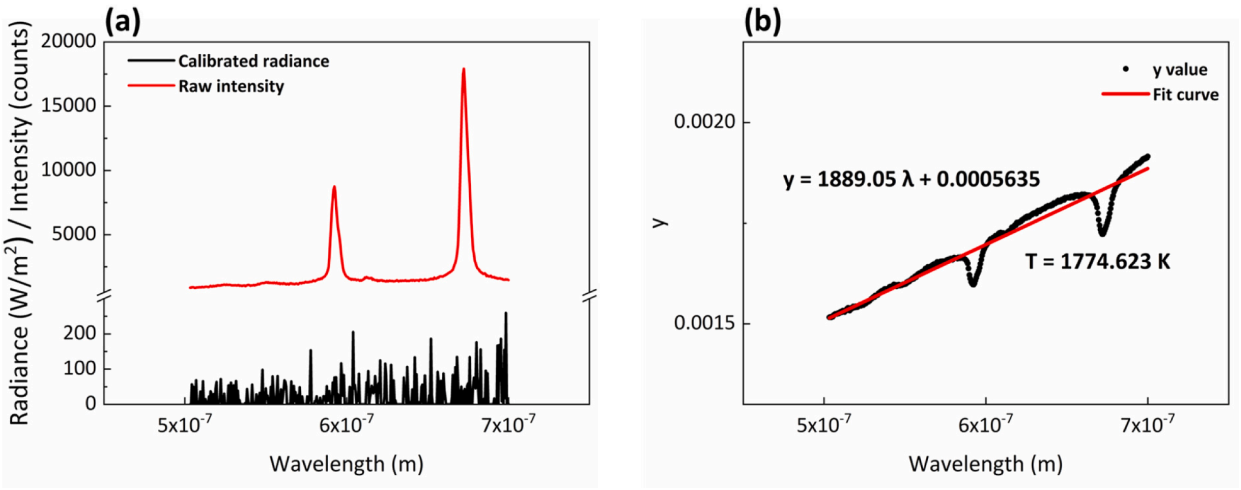


**Fig. 6.** Raw radiation intensity signal from the spectrometer and calibrated radiance (a); the derived quantity y from this intensity as a function of the wavelength (b), for ECSP-M5 burning at 0.1 MPa.

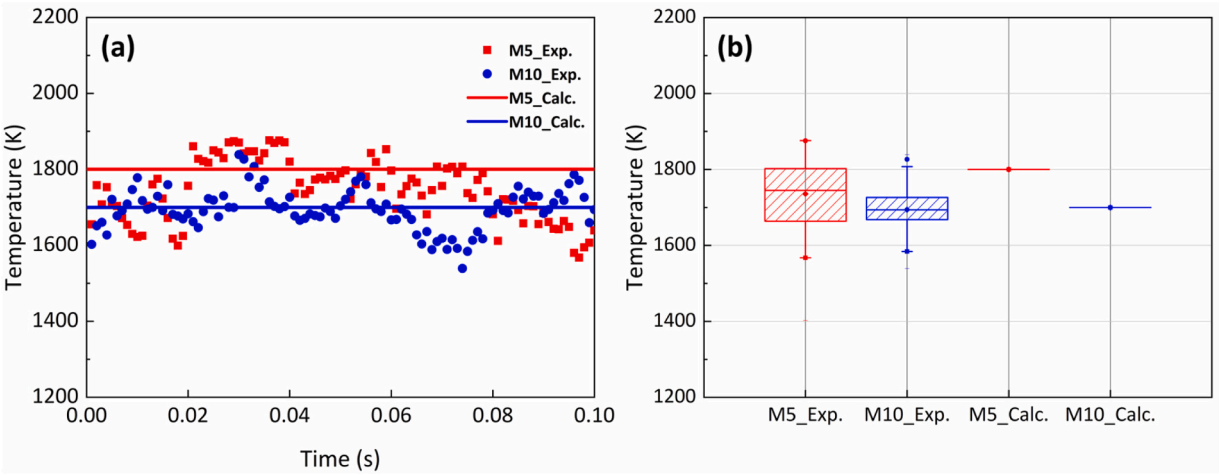


**Fig. 7.** Time-resolved temperature distribution (a) and average combustion temperature shown as box plot (b), during combustion of ECSP-M5 and ECSP-M10 at 0.1 MPa and 300 V and 1 A, in comparison to their corresponding theoretical adiabatic combustion temperatures obtained from Cheetah 4.0, shown as straight lines.

thermal conductivity with metallized propellants have a favorable impact on their combustion rates in the considered pressure range, as shown next.

Pyroelectric combustion images of all ECSPs were captured in 0.1 to 2.0 MPa pressure range using the Phantom camera. In general, when the electrical power was applied initially, the propellant started to conduct power from the top positive electrode to the bottom negative electrode, at the onset of current signal rise ($t_1$). Liquid bubbles were observed on the propellant surface near the top electrode, followed by ignition and later combustion with continuous supply of the electrical power. In this study, combustion occurred preferentially at the positive electrode with these ECSPs, however it was reported to occur on either electrode depending on parameters such as current density, electrode area ratio, electrode surface roughness and electrode polarity by a previous work [10]. Products gases from propellant combustion were redirected sideways at the top electrode. However, this does not affect the steady state combustion of these propellants, as observed through combustion images from which their combustion rates are deduced. Furthermore, the initial shape of these propellants remained intact during their combustion process and the combustion surface was not affected by the vertical downward force caused by the action of gravity of the positive electrode. There was no additional measurement error of combustion rates associated with the vertical burning configuration since this configuration was maintained the same for all tests conducted in the present study.

Pyroelectric combustion mechanisms and global reaction processes of LP/PVA/water mixtures and ECSPs were elucidated in detail in our recent study performed at ambient pressures [17], wherein the influence of external electrical power on the combustion behaviour of ECSPs was investigated. It involves electrochemical decomposition of ionic oxidizer coupled with thermochemical reactions between the oxidizing species generated from the former and the fuel species. Briefly, when the electric power is applied to the propellant, the global electrolytic process between LP and water occurs and generates substantial amount of oxidizer species. This species would now react with fuel species from thermal decomposition of PVA, to create products such as $CO_2$, $H_2O$, LiCl, etc. along with a corresponding heat release through thermochemical reactions [11]. With metallized ECSPs, the oxidizer species from electrolytic decomposition would react with fuel species from PVA decomposition as well as W to generate $WO_3$ in the metal oxidation process, in addition to the above products. This metal oxidation occurs typically in the condensed phase followed by some gas phase reactions. In addition, the flow of electrons across the propellant generates thermal energy through Joule heating [5], which also initiates certain extent of reactions between the oxidizer and fuel.

Pyroelectric combustion rates are obtained from combustion images for different ECSPs in the pressure range of 0.1-2.0 MPa and presented in

Fig. 8. Here, open symbols were used to show small error bars/deviation of burning rates (of each sample), which was noticed for a significant number of repeat tests, and to explicitly indicate the actual number of repeat tests that were performed at each pressure. The small error bars (deviation) in each of the datapoints suggest that these samples exhibited steady burning across their entire cross section in each test. On the other hand, a large difference in burning rates among repeat points could be due to considerable batch to batch variation of samples caused during their preparation and/or curing stage. Overall, combustion rates for each composition indicate a significant increment with increase in pressure in the entire test range and followed St. Robert's burn rate law. For ECSP-M0, combustion rates have increased linearly from 2.25 mm/s at 0.1 MPa to 7.54 mm/s at 2.0 MPa pressure in a log-log plot with a correlation of 87% and an increment of 3.2 times in the tested range. The pressure exponent $n$ of 0.39 indicates that this propellant is highly stable in terms of its pressure sensitivity in the considered range. At high pressures (2.0 MPa), burning particles and gases emerging from propellant decomposition are located close to the burning surface, which promotes accumulation of heat from the flame near the surface of propellant. In addition, the thermal heat feedback from the flame/combustion products to the unburnt propellant surface is improved thus further enhancing thermochemical reactions. This is seen as highly luminous combustion zone with ECSP-M0 burning at elevated pressures in Fig. S2 of the supplementary. Improved rate of heat feedback to the unburnt propellant surface causes high heat release rate from propellant burning and in turn enhanced combustion rates. Since thermochemical reactions are greatly coupled with electrochemical reactions, which are essential for electrolytic decomposition of ionic oxidizer during propellant combustion, there is always a combined effect from electrochemistry and thermochemical reactions in augmenting combustion rates of ECSP-M0 at elevated pressures.

Inclusion of W to ECSP-M5 improved combustion rates marginally at high pressure (2.0 MPa) relative to ECSP-M0 as seen in Fig. 8a. For ECSP-M5, combustion rates increased linearly by 4.1 times from 1.87 mm/s at 0.1 MPa to 7.64 mm/s at 2.0 MPa with a correlation of 86%. Similarly, an increment of combustion rates by 4.3 times and 3.3 times are observed for ECSP-M10 and ECSP-M15 respectively, in the 1.0-2.0 MPa range. These combustion rates for different ECSPs and their correlation coefficients are presented in Table 3. Addition of W up to 10% in ECSP formulations does not have a significant influence on combustion rates in the considered pressure range, relative to the baseline ECSP-M0. Further, variations in combustion rates of these ECSPs at each pressure are within the spread of these data. Similarly, disparity in the combustion temperature from pyrometry noticed between ECSP-M10 and ECSP-M5 was within the error band as well. This is because these formulations have either oxidizer-rich or fuel-rich equivalence ratios on either side of the actual stoichiometric value (Table 2).

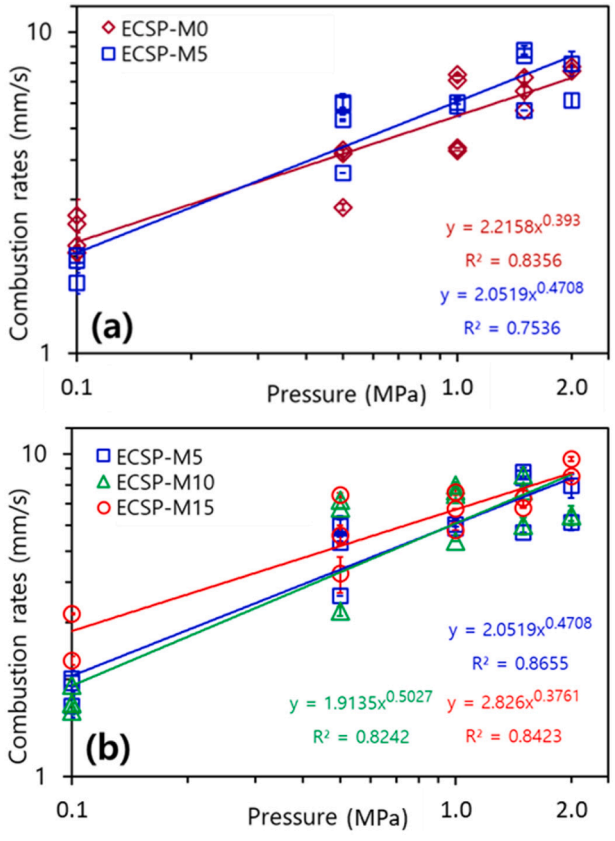


**Fig. 8.** Pyroelectric combustion rates as a function of pressure for metallized ECSPs in comparison to baseline ECSP at 300 V and 1 A.

It is obvious that increasing the metal content in the conventional solid propellant combustion reduces the burning rate. In the conventional solid propellant, the coarse ammonium perchlorate (AP) particles are replaced with the metal additives which enlarge the space between the adjacent AP particles thereby limiting the interaction of the leading edge flame with AP particles which further leads to the decrease heat feedback from the flame [23]. This results in the reduced burning rate. Also, the chances of metal accumulating and forming the sintered bed on the solid surface acts as a heat sink resulting into reduced heat feedback to the surface as the part of the heat from the flame is taken by the metal sintered bed for melting and burning away from the solid surface [24, 25]. The increased metal additive reduces the number density of the leading edge flame which gives rise to reduced localized flame hot spots for proper heat feedback, and therefore the burning rate reduction is seen.

But in the case of ECSP, the burning is not self-sustained after the initial ignition as opposed to the case of the conventional solid propellant where the initial ignition drives the whole combustion without any external intervention. In ECSP, one needs to supply the constant electrical power for sustaining the burning of solid propellant. Metals are efficient electrical conductor, which means for constant power supply, increasing the metal content should enhance the conduction, and the burning rate should increase linearly with respect to the amount of the metal content. The effect of electrical conductivity is much pronounced in the 15% content than the reduced heat feedback due to high metal content. The elaborative study on this is beyond the scope of this paper, and thus herein the experimental data collected are reported.

However, with ECSP-M15, combustion rates are considerably higher than that of those with other ECSP formulations at each pressure, as seen in Fig. 8b. For instance, an increment of 46.5% is noticed for ECSP-M15 relative to ECSP-M5 at 0.1 MPa, whereas it is 18.5% between these two formulations at 2.0 MPa. The presence of large content of metal particles increased the bulk thermal conductivity of this propellant that enhanced the heat transfer rate from the flame/combustion zone to the unburnt propellant surface, thus increasing combustion rates. However, this enhancement in the performance is more conducive to the pressure effect, which would tend to dominate further at even high pressures beyond 2.0 MPa. In other words, the augmentation obtained in combustion rates due to increase in W content is relatively diminished at high pressures ($>$ 2.0 MPa), since the heat accummulation effect from near surface location of the combustion zone predominates the thermal conducvity effect, in significantly improving the electrolytic decomposition and thermo-chemical reactions involved in pyroelectric combustion of ECSPs.

Combustion rates from this study are on the same order of the results reported in a previous work on LP based ECSPs with Al as metal additive [9], although the experimental test conditions and propellant formulations were not exactly similar between these studies. It was illustrated that Al based ECSPs with 15% metal content improved combustion rates up to 4 mm/s at 160 V and 2.0 MPa. In the present study, W based ECSP-M15 exhibited combustion rate increments up to 9 mm/s at 2.0

MPa pressure with the external voltage of 300 V. This suggests that addition of W in ECSPs also promotes considerable enhancement in combustion rates when compared to the baseline case, although this aspect was not discernible from theoretical performance calculations in Section 3.1. Thus, the present study affirms that the influence of W on ignition and combustion characteristics of ECSPs has a favorable impact in the propellant performance, which is further augmented at high pressures.

## 4. Conclusions

In this study, the ignition and combustion characteristics of LP/PVA based metallized ECSPs, at three different tungsten (W) contents of 5%, 10, and 15%, were investigated in comparison to the non-metallized baseline propellant. Ignition delay time, minimum electrical energy required for ignition, combustion temperature and combustion rates of these propellants were obtained experimentally in the pressure range of 0.1-2.0 MPa, using techniques such as multi-wavelength pyrometry and combustion photography. Measurements of current, voltage, and radiation intensity from the propellant flame were also recorded using digital oscilloscope. Furthermore, thermochemical equilibrium calculations were performed for W-based ECSPs to compare their performance parameters with the baseline case.

Results inferred that the presence of W in ECSPs reduced the theoretical adiabatic combustion temperature and specific impulse of these propellants. This is due to increased oxygen requirement for W oxidation with increasing fuel-rich stoichiometry of ECSPs and increase in condensed phase products. However, the addition of W to ECSPs induced considerable improvement in their ignition characteristics and combustion rates at high level of metal content (15%). Furthermore, increase in pressure decreased the ignition delay time ($T_{ign}$) and minimum electrical ignition energy significantly for all ECSPs, regardless of the presence of W in their formulations. Similarly, inclusion of W also reduced $T_{ign}$ and electrical ignition energy for different ECSPs, at each pressure level. In addition, pyroelectric combustion rates were increased substantially by 3-4 times with increase in pressure for each composition. However, the pressure effect caused by closer location of combustion zone to unburnt propellant surface is observed to be more dominant than the metal addition effect through increased electrical and thermal conductivity with these propellants, in enhancing their performance parameters.

## CRediT authorship contribution statement

**Kanagaraj Gnanaprakash:** Investigation, Methodology, Formal analysis, Writing – original draft. **Daehong Lim:** Data curation, Visualization. **Jack J. Yoh:** Conceptualization, Investigation, Supervision, Writing – review & editing, Funding acquisition.

## Declaration of Competing Interest

The authors declare that they have no known competing financial interests or personal relationships that could have appeared to influence the work reported in this paper.

## Data Availability

No data was used for the research described in the article.

## Acknowledgments

This work was funded by the National Research Foundation of Korea (Project Grant No. NRF- 2020R1I1A1A01065097) contracted through IAAT and IOER at Seoul National University.

## Supplementary materials

Supplementary material associated with this article can be found, in the online version, at doi:10.1016/j.tca.2022.179421.

## References

[1] A.T. Hiatt, R.A. Frederick, Laboratory experimentation and basic research investigating electric solid propellant electrolytic characteristics, in: Proceedings of the 52nd AIAA/SAE/ASEE Joint Propulsion Conference, AIAA paper 2016-4935, Salt Lake City, Utah, US, 2016.
[2] C. Grix, A. Katzakian, D.C. McGehee, Electrically controlled solid propellant, US Patent 0011276, 2006.
[3] W.N. Sawka, M. McPherson, Electrical solid propellants: A safe, micro to macro propulsion technology, in: Proceedings of the 49th AIAA/ASME/SAE/ASEE Joint Propulsion Conference, AIAA paper 2013-4168, San Jose, California, US, 2013.
[4] Z. He, Z. Xia, J. Hu, L. Ma, Y. Li, Thermal decomposition and kinetics of electrically controlled solid propellant through thermogravimetric analysis, J. Therm. Anal. Calorim. 139 (2020) 2187–2195.
[5] J.K. Baird, R.A. Frederick Jr., Thermochemistry of combustion in polyvinyl alcohol + hydroxyl ammonium nitrate, Aerospace 8 (5) (2021) 142.
[6] M.S. Glascock, J.L. Rovey, K.A. Polzin, Impulse and performance measurements of electric solid propellant in a laboratory electro-thermal ablation-fed pulsed plasma thruster, Aerospace 7 (6) (2020) 70.
[7] L. Bao, W. Zhang, X. Zhang, Y. Chen, S. Chen, L. Wu, R. Shen, Y. Ye, Impact of MWCNT/Al on the combustion behaviour of hydroxyl ammonium nitrate (HAN)-based electrically controlled solid propellant, Combust. Flame 218 (2020) 218–228.
[8] S.Z. Wang, J.Y. Lyu, W. He, P.J. Liu, Q.L. Yan, Thermal decomposition and combustion behavior of ion conductive PEO-PAN based energetic composites, Combust. Flame 230 (2021), 111421.
[9] Z. He, Z. Xia, J. Hu, Y. Li, Lithium-perchlorate/polyvinyl-alcohol-based aluminized solid propellants with adjustable burning rate, J. Propuls. Power 35 (3) (2019) 512–519.
[10] Y. Li, Z. Xia, J. Hu, L. Ma, X. Na, Z. He, Experimental investigation of the ignition and combustion characteristics of electrically controlled solid propellant, Acta Astronaut. 184 (2021) 167–179.
[11] K. Gnanaprakash, M. Yang, J.J. Yoh, Thermal decomposition behaviour and chemical kinetics of tungsten based electrically controlled solid propellants, Combust. Flame 238 (2022), 111752.
[12] L. Brunacini, Investigation of the electrical resistivity of a perchlorate oxidizer based electric propellant formulation, MS Thesis, Arizona State University, Arizona, US, 2018.
[13] D. Sundaram, V. Yang, R.A. Yetter, Metal-based nanoenergetic materials: synthesis, properties, and applications, Prog. Energy Combust. Sci. 61 (2017) 293–365.
[14] L. Bao, H. Wang, Z. Wang, H. Xie, S. Xiang, X. Zhang, W. Zhang, Y. Huang, R. Shen, Y. Ye, Controllable ignition, combustion and extinguishment characteristics of HAN-based solid propellant stimulated by electric energy, Combust. Flame 236 (2022), 111804.
[15] I. Zamir, M. Ben-Reuven, A. Gany, D. Grinstein, Investigation of electrically controlled ammonium nitrate-epoxy solid propellant at high pressures, Propel. Explos. Pyrotech. 46 (2021) 477–483.
[16] M. Mohsin, A. Hossin, Y. Haik, Thermal and mechanical properties of poly (vinyl alcohol) plasticized with glycerol, J. Appl. Poly. Sci. 122 (2011) 3102–3109.
[17] K. Gnanaprakash, J.J. Yoh, Understanding the pyroelectric combustion behaviour of metallized electrically controlled solid propellants, Proc. Combust. Inst. (2022), https://doi.org/10.1016/j.proci.2022.07.036. Article in press.
[18] J.K. Baird, J.R. Lang, A.T. Hiatt, R.A. Frederick, Electrolytic combustion in the polyvinyl alcohol plus hydroxyl ammonium nitrate solid propellant, J. Propuls. Power 33 (6) (2017) 1589–1590.
[19] K. Gnanaprakash, Y.H. Lee, J.J. Yoh, Investigation of aging induced processes on thermo-kinetic and combustion characteristics of tungsten pyrotechnic delay composition, Combust. Flame 228 (2021) 114–127.
[20] N. Daniel, G. Fralick, Use of a multi-wavelength pyrometer in several elevated temperature aerospace applications, Rev. Sci. Inst. 72 (2) (2001) 1522–1530.
[21] M.R. Weismiller, J.G. Lee, R.A. Yetter, Temperature measurements of Al containing nano-thermite reactions using multi-wavelength pyrometry, Proc. Combust. Inst. 33 (2) (2011) 1933–1940.
[22] L.E. Fried, W.M. Howard, P.C. Souers, Cheetah 2.0 User's Manual, UCRL-MA-117541 Rev. 5, Lawrence Livermore National Laboratory, California, US, 1998.
[23] K. Jayaraman, K.V. Anand, S.R. Chakravarthy, R. Sarathi, Effect of nano-aluminium in plateau-burning and catalyzed composite solid propellant combustion, Combust. Flame 156 (8) (2009) 1662–1673.
[24] J.K. Sambamurthi, E.W. Price, R.K. Sigman, Aluminum agglomeration in solid propellant combustion, AIAA J. 22 (8) (1984) 1132–1138.
[25] B. Kathiravan, C. Senthilkumar, R. Rajak, K. Jayaraman, Mean burning rate variation in composite propellant combustion due to longitudinal acoustic oscillations, J. Propuls. Power 36 (4) (2020) 604–616.